LABORATORY EXPLOSIVE TESTING AT SMALL SCALE

Leslie C. Taylor, William E. Fourney, H. Ulrich Leiste
Dynamic Effects Laboratory
University of Maryland
College park, MD 20742

Small scale testing has proved very useful in exploring the details of buried charge target loading mechanisms. If the target is of reasonable size relative to the charge, the target is loaded in two steps or phases. It has been possible to gain insight into the density distribution in the soil cap that provides the first phase of the target loading. This is expected to be quite useful in validating computational models of the loading. The actual load on a target by the explosion of a buried charge has a significant non-deterministic element. Small scale testing enables one to run enough nominally identical tests to develop sound estimates of the nondeterministic part of the target loading. It appears that both the mean and the standard deviation of this loading are scalable to other charge sizes.

INTRODUCTION

The design of vehicles resistant to the explosion of buried charges should be based on an understanding of the physics of in-soil explosions and how the explosion products interact with the target. In considering the physics of buried explosive charges, the effect of buried charges on targets and improving our understanding of the target loading process, well instrumented, small scale explosive testing in a laboratory setting has proved to be very useful and will continue to do so. Small scale testing is, in fact, uniquely able to provide insight into these processes. Full scale explosive testing is very expensive and because of its scale, visualization and instrumentation can be difficult. Small scale explosive testing is more cost-efficient, more easily observed and more easily documented. Importantly, small scale explosive testing is economical enough that individual tests can be repeated enough times to produce statistically significant results in the investigation of non-deterministic processes and effects.

The Dynamic Effects Laboratory at the University of Maryland (UMD) has conducted a very large number of small-scale explosive tests in which the charge was buried in water-saturated sand. The general objective has been to develop information that will enable designers to develop more blast resistant vehicles. The testing has encompassed measurement of the pressure loading at various locations on the target and visualization of the ejecta from a buried explosion and its impact on a target as well as measurement of total vertical impulse on the target. Water-saturated sand was the medium chosen for the tests described in this paper. McAndrew 2008, e.g., show the total impulse on the target increasing with increasing soil moisture. In many of our tests, the objective was to determine the pressure on the surface of a "non-deforming" fixed target as a function of time and position.

Small scale testing has been shown to be able to accurately predict the results of full scale tests. The target *above* a buried explosion is loaded by soil driven by the expanding gasses of the explosion. In effect, the target is loaded by an explosively formed projectile (EFP) made of soil. The direct effect of the shockwave on the target is negligible, unless the target is in good contact with the ground: e.g., a tank track. Hence, the loading of a target above a buried explosion is a bubble driven process, not a shockwave process. Never the less, both the explosive effects and that response of the target can be scaled in a relatively simple fashion using Hopkinson ($W^{1/3}$) scaling. Figure 1 shows a comparison of two series of tests: The full scale tests were conducted with 2.3 kg (5 lb) and 4.5 kg (10 lb) charges; the small scale tests, with 0.609 g charges. Clearly, the large scale results can be accurately enough predicted from the small scale test results using Hopkinson scaling.
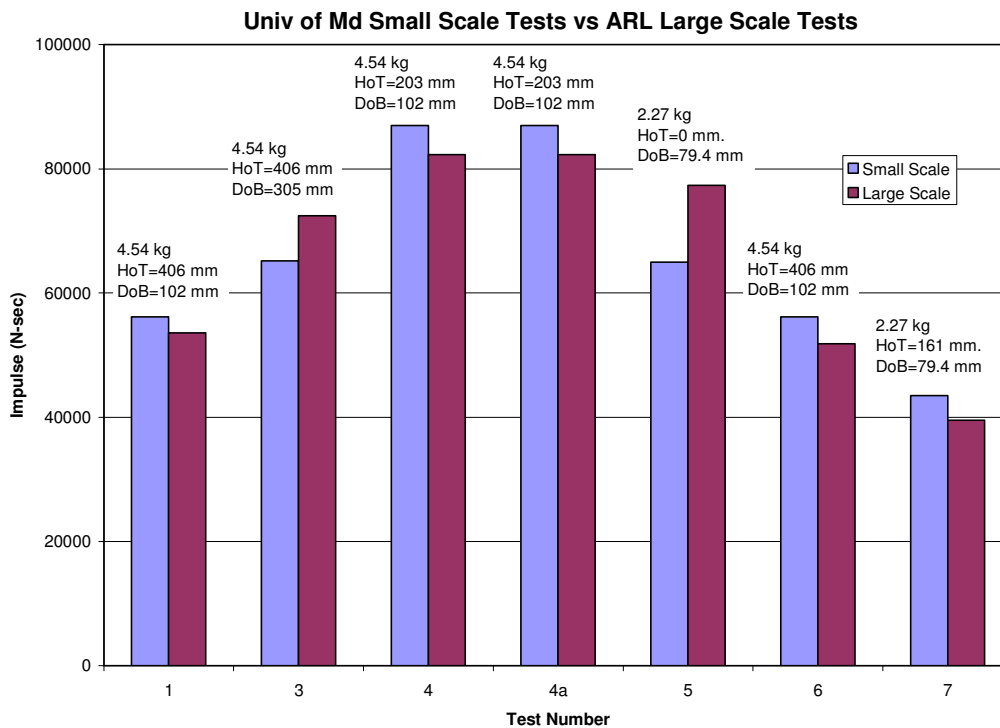

Figure 1 Comparison of Total Vertical Impulse for Small and Large Scale Tests

TEST METHODS

The data used in this paper came from tests conducted at a quite small scale. In these tests we used Detasheet charges. By far, most of the tests were conducted with 4.4 g charges. The Detasheet contained 63% PETN and 37% plasticizer. Nearly all of the charges were detonated using RP-87 detonators manufactured by Reynolds Industries. These charge weights include only the mass of PETN in the Detasheet plus the mass of explosive in the detonator. They do not include the mass of the plasticizer.

The charges generally had a diameter to height ratio of about 1.7. In all cases, the explosive was contained in a thin-walled plastic cylinder as shown in Figure 2, so as to minimize confinement by the case.

All tests were conducted in an indoor test facility in the Dynamic Effects Laboratory. Figure 3 shows an overall view of the test bed. The saturated sand was contained in a 1.5 m X 1.5 m X 0.6 m deep steel tank. The bottom of the tank was covered with rocks and a cloth mesh was placed over the rocks. The volume above the cloth mesh was filled to the desired level with HD-2 sand which was purchased at Home Depot. The properties of this sand are described in Fourney 1999. Piping to the underside of the tank allows the test bed to be evenly saturated with water from below. The saturation system uses a standpipe to move water into the underside of the tank and upwards into the sand bed. Very low pressure is used to ensure that saturation of the sand bed is uniform.

Figure 2 Typical Deta Sheet Charge
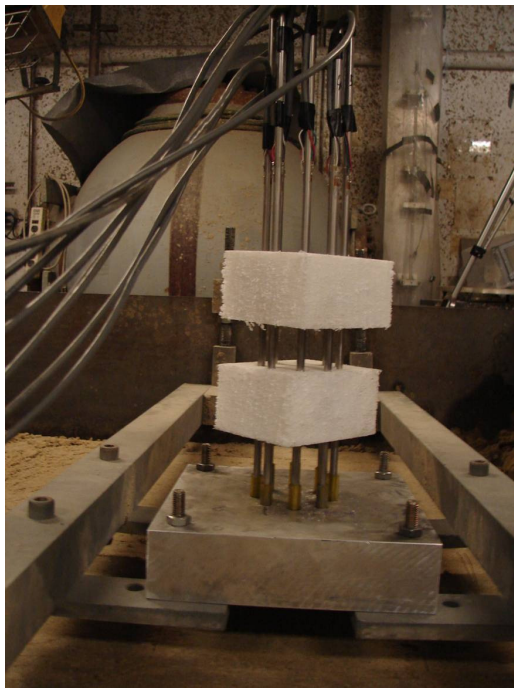

Figure 3 Explosive Test Facility at UMD

Figure 4 Typical Kolsky Bar Setup

For pressure measurements, the targets were non-deforming plates, rigidly attached to the tank. The pressures were measured using Kolsky bars mounted in the plate. The strain gages on the Kolsky bars were mounted on opposite sides of each of the bars and used in a Wheatstone bridge to minimize the effect of bending of the bars. Initially, the Kolsky bars were located in a line starting at the center of the plate, directly above the explosive charge and at various distances from the center. Later, a circular arrangement was used as shown in Figure 4. All of the Kolsky bars used in all of the tests discussed in this paper were 6.35 mm (0.25 in.) in diameter.

TARGET LOADING MECHANISMS

The interaction between buried charges and targets of interest takes place in the near field of the explosion. This means that details of the charge shape, local soil properties and geometry, etc. are important. However, even when all of the dimensions of the explosive – target geometry are kept constant, the local pressures on the target are not truly repeatable. This lack of repeatability not only causes significant shot – to – shot variation in the pressures measured at any given point on the target; the pressures are not even axially symmetric within a single shot Taylor et al 2010. The effect of this randomness is discussed later.

The "soil cap" over the charge is propelled at the target by the expanding bubble of gas from detonation of the explosive. Impact of this soil cap is a major contributor to the load on the target, especially to the pressures on and near the centerline of the charge, where the loads are greatest. The properties of the soil cap, *when it impacts the target*, are therefore very important. However, the properties and configuration of the soil cap are modified from their pre-blast state by the time it hits the target.

The thickness of the dome of soil hitting the target varies in time and position, both radially and vertically. When the charge detonates, it first emits a shockwave. Because of the shape of the buried charges of interest, e.g., a high diameter to thickness ratio, and the location of the detonator, usually in the center of the base of the charge, the shape of the shockwave entering the soil near the center of the charge is more or less parallel to the upper face of the charge. Farther from the center of the charge, the shock front is more curved. When the shockwave from the explosion reaches the surface, the impedance mismatch with the air causes its reflection back into the soil cap, causing the material of the soil cap to cavitate. Further reflection from the back of the soil cap, i.e., the expanding explosion gas bubble, can cause the cavitated region to collapse. Thus, the density distribution in the soil cap that hits the target changes continuously as it rises and is a complex function of the (variable) speed of sound in the soil cap, the depth of burial (DoB) of the charge (i.e., the initial thickness of the soil cap) and the height of the target (HoT) above the soil surface.

Figure 5: Spray from 0.8g Charge Detonated in Saturated Sand (Video Image: ~16.76μs after firing)

However, not all of the shockwave energy is reflected at the soil surface. A weak shock is emitted into the air and spray from the surface of the soil is thrown upward. This soil surface is launched upward, forming a dome, at an initial velocity equal to about twice the particle velocity due to the shockwave when the shockwave reaches the surface. Figure 5 shows spray being thrown off the surface and the beginning of the formation of the dome. The DoB is 5.7 mm, equivalent to a DoB of 10 mm for a 4.4g charge.

At some distance below the surface of the soil, the negative pressure in the relief wave interacts with pressure in the soil to reduce the local absolute pressure to zero. The pressure in the soil cap at any point, before it is reduced by the relief wave, is the atmospheric pressure plus the weight of the soil above that depth plus the pressure in the tail of the shockwave. In water, where the phenomenon can be photographed: "Underwater photography has shown that the cavitated region consists of bubbly water, resembling soda water. This process is called *bulk cavitation*. At the first moment of its formation, the cavitated region is of considerable horizontal length and substantially smaller, but finite thickness" Snay 1970. Bulk cavitation in a fluid is akin to spalling in a solid material. In a medium such as saturated sand, which has little cohesive strength, bulk cavitation has the effect of locally reducing the density of the cavitated region to a very low value.

If the charge is sufficiently deeply buried, the rising soil cap still may have a distinct cavitated region when it hits the target. In the absence of other effects, the soil above the cavitated zone may have nearly the same density as the undisturbed soil. Below that is a cavitated zone, whose thickness varies with time and radial position and below that, another layer containing soil at a higher density. The material density in the cavitated zone is theoretically zero, but in actual practice, it is just very low in this zone.

When the soil cap hits the target, it can produce a non-uniform pressure rise if a cavitated (low density) region is present. Figure 6 shows two pressure vs. time curves from the same test. In Figure 6a, where the gage was directly above the center of the charge, the pressure rises in a single sweep to its peak. In Figure 6b, where the gage was 12.7 mm from the center of the charge, there is a step or hesitation in the pressure rise. We believe this is due to bulk cavitation: i.e., a layer of reduced density in the rising soil cap. Also, a small "precursor" pressure step of about 42 mPa, seen before the primary pressure rise in Figure 6a, arrives 0.285 ms after firing. The precursor may be caused by the spray from the surface. The spray from the surface of the soil cap is one of the effects of the shockwave's hitting the soil surface as noted above.
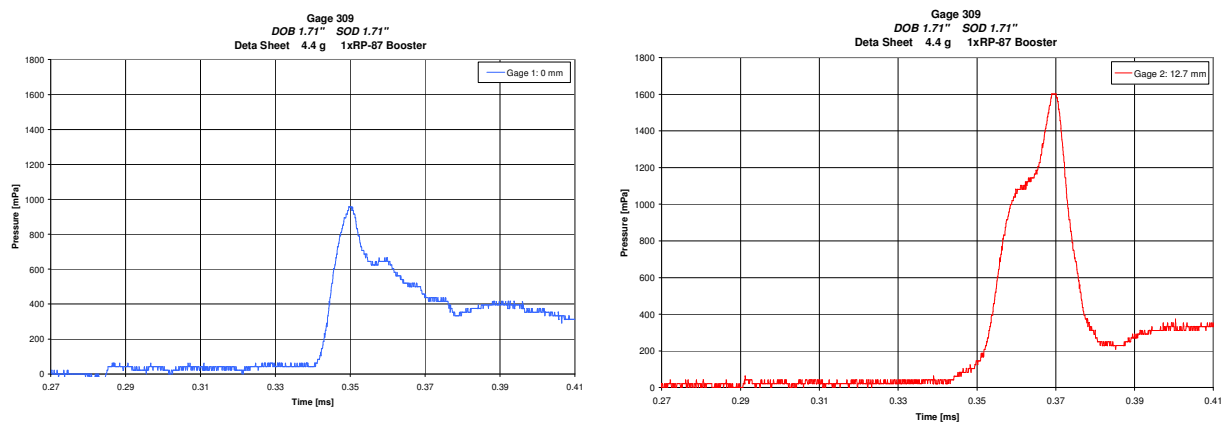

Figure 6   Pressure vs. Time DoB = 43.43 mm, HoT = 43.43 mm
a. Kolsky Bar Centered Above Charge   b. Kolsky Bar 12.7 mm off Center of Charge

A second process that modifies the soil cap before it hits the target is Richtmyer -Meshkov Instability (RMI). RMI occurs when an incident shock wave accelerates an interface between two fluids of different densities and thus amplifies any initial perturbation on the interface

Palekar 2007. Our interest here is amplification of the "initial perturbations." If the shockwave proceeds from a dense fluid, i.e., water-saturated sand, into a less dense fluid, i.e., air, RMI will manifest itself as spikes of the heavy material penetrating into the light fluid. It is initiated when the interface between the two media is not smooth. This is precisely the case with the surface of any soil. The soil surface is always non-smooth at some scale, from tire tracks and pebbles down to sand grains. Thus the interface between the soil and the air is always irregular or "perturbed."

Figure 7: Sand Dome - 0.8g Charge in Saturated Sand (Image 3.5 μs After Figure 3)

RMI is the origin of spikes of material that then move faster than the bulk of the soil cap. Figure 5 shows these spikes beginning to form. Figure 7, imaged 3.5 μs after Figure 5, shows them at a more developed stage, as well as smaller spikes developing on the periphery of the larger ones above and nearer the center of the charge. The spikes appear to form first at the base of the small cavities in the surface of the soil that are the inevitable consequence of its granularity. The development and growth of RMI spikes are not well understood at this time. However, since the smoothness of the surface of the soil is chaotic, in the sense that it cannot be explicitly specified, RMI ultimately manifests itself as a chaotic distribution of spikes moving at higher speeds than the bulk of the soil cap. Since the pressures being measured on the surface of the target are impact (stagnation) pressures, this leads directly to the circumferential randomness of the peak pressures at any radius from the center of the charge, as discussed later in this paper.

Simple spherical spreading of the soil cap also affects the properties of soil cap that hits the target. As Figure 7 shows, the soil cap very quickly assumes the shape of a very rough hemisphere or dome. Bergeron 1998, using flash X-rays, showed that the dome is hollow and presumably filled with gaseous explosion products. The dome not only rises to hit the target above it, it, at first, remains continuous with the as yet undisturbed surface and increases somewhat in diameter as it rises. The rate of increase in diameter appears to be relatively small compared with its rate of rise. This increase in diameter has the effect of thinning the soil cap, Bergeron 1998, as the material in it is spread over the surface of a hemisphere larger in diameter than the charge, much as the thickness of a balloon decreases as it is inflated. This shortens the period of peak loading on the target. Notice in Figure 8a, the initial, high pressure loading period is quite short, suggesting a thin soil covering over the bubble of gaseous explosion products. The increase in soil cap thickness due to cavitation and its thinning due to spherical spreading are competing processes.

All of the above processes happen very quickly, very early in the loading process. These processes are followed by two additional processes which load the target over a much longer time. These pressures are much lower, but because of their long duration and large area of influence, their contribution to the total impulse is significant if the target is large enough compared to the charge.

Material outside the radius of the soil cap is scooped out of the crater by the gaseous explosion products and travels upward essentially parallel to the instantaneous wall of the crater being excavated, before it hits the target. This forms an annular stream or jet of material which hits the target. This impact is not normal to a flat target plate. Recall that in the initial target strike, the material hitting the target had a very high velocity normal to the target or soil, but a relatively low horizontal velocity. In this stage of loading, the vertical and horizontal velocities appear to be comparable.

Under these conditions, the local rate of pressure rise on the target is slower, the peak pressure is much lower and the shape of the pressure – time trace is irregular and variable, but of much longer duration. The longer duration of high pressure appears to be the result of thickening of the wall of material making up the annulus of material coming out of the crater. In effect, there is an expanding circular stagnation ring where this material hits the target. Figure 8 shows the difference in the shape of the pressure – time curves between this process and the initial impact. Note the difference in pressure and time scales in Figures 8a and 8b.
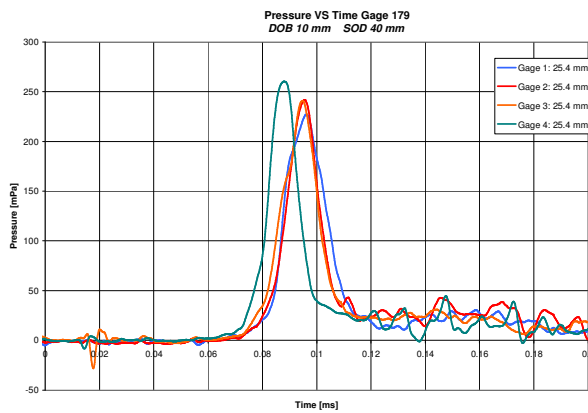

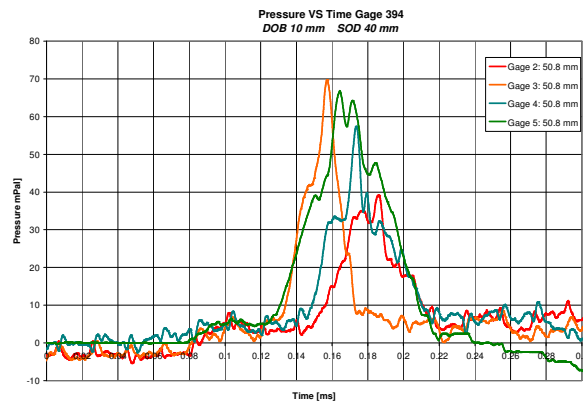Figure 8a Typical Pressure – Time traces for R=25.4 mm

Figure 8b Typical pressure – Time Traces for R=50.8 mm

.
At R = 25.4 mm, within the earlier phase, the duration of the pressure pulse is about 0.03 ms and the peak pressures are 220 to 260 mPa. At R = 50.8 mm, the peak pressures are 40 to 70 mPa and the duration is about 0.1 ms, over three times as long.

The annulus of soil being excavated from the crater and stagnating on the plate as the crater grows can also provide confinement of the gaseous explosion products between the crater and the bottom of the plate, which then allows the gas bubble to provide an upward force due to overpressure, so long as the gage pressure under the target plate is positive. We believe this pressure is the "tail" of the pressure – time curve that trails to the right in Figures 8a and 8b. In spite of the lower pressures from the gas bubble and from the impact of the material being excavated from the crater, if the target is big enough, these processes can make a significant contribution to the total impulse because of their long duration and wide area of application.
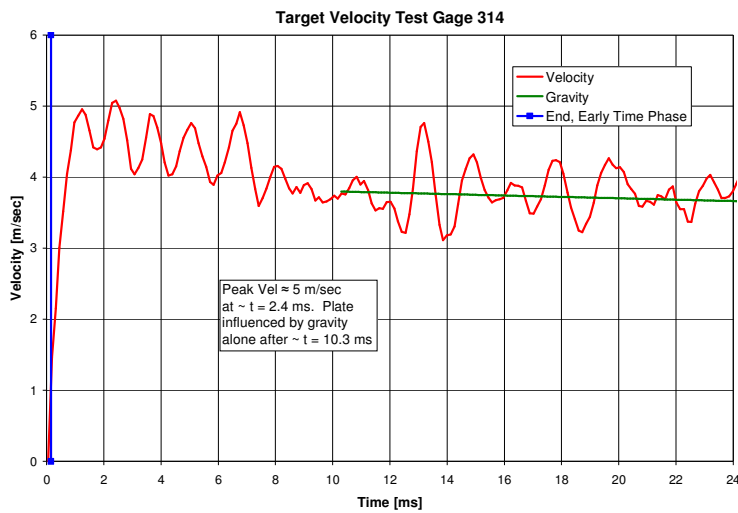
Target Velocity Test Gage 314

Figure 9 shows the vertical velocity of a target plate as a function of time. In this case the target was 0.483 m. in diameter, a quite large target. The HoT and DoB were the same as those in Figure 8. It shows that the plate continues to gain velocity for about 2.4 ms. All of the increase in velocity after about 0.15 ms, shown by the blue line in Figure 9, over 50% of the total velocity, was due to these latter two processes, in this case.

Figure 9 Target Velocity as Function of Time

DENSITY DISTRIBUTION IN THE SOIL CAP

The first *significant* loading event on the target is the impact of the soil cap made up of the soil immediately above the explosive. This initial loading is very concentrated in space and time. As stated earlier, the soil cap is a very crude EFP made of soil. Further, the properties of this soil cap, particularly the density, are not the pre-detonation, *in situ*, soil properties. The density of the soil is no longer uniform through the thickness of the soil cap by the time it hits the target, what ever its height. The distribution of density in the soil cap varies as a function of time and with position in the moving soil cap. Actually measuring the density distribution in the soil cap is very difficult, if not impossible, at this time. However, it is possible to infer the density distribution *at the time of impact* with a target from the pressure time data. The pressure vs. time curve, at any point on the target where the impact is essentially normal to the target, carries information about the density and its distribution in the material that impacted the target.

A few simple observations enable the density distribution along the centerline of the soil cap to be estimated. First, the *initial* pressure loading on the target at or near the centerline of the charge is an impact load. Further, the impacting material, a sand - water - air mixture, can be treated as a fluid. This is reasonable since saturated sand has little cohesiveness and the velocity of the material initially hitting the target is very high (typically, 500 to 1000 m/sec), so that what little cohesive strength the material has is irrelevant. Second, since the target in the cases discussed below is a flat plate normal to the flow of the material impacting it, the pressure on the target is the stagnation pressure and Bernoulli's equation applies:

$$p = \tfrac{1}{2}\,\rho V^2$$

In this equation, p is the stagnation pressure, ρ is the density of the material and V is its velocity. Given this equation, it is quite simple to determine the product ρV^2 from the pressure data. The difficulty is separating the density from the velocity in this product.

To do this, we observe that the *average* velocity of the material initially hitting the target is simply the distance from the surface of the soil to the target (HoT) divided by the time of arrival (ToA) of the pressure pulse. Then, we must determine when the impact process ceases to be significant, i.e., when the back of the soil cap has reached the target. This last is important since the thickness of the soil cap is continuously changing, due to the effect of bulk cavitation as it rises toward the target, i.e., the back of the soil cap travels more slowly than the front. Therefore we must also know the velocity of the back of the soil cap. The velocity difference between the front and the back of the soil cap can be thought to be analogous to stretching of a conventional EFP. The thickness of the soil cap is also trying to decrease due to spherical spreading as it rises. Determining the end of the impact phase is more difficult than determining the start because the transition from impact loading to the pressure loading on the target described above is not always obvious. In Taylor 2011, it was done by inspection of the relevant pressure – time curves.

At this time there does not seem to be any experimental data that would allow one to determine the form of the velocity gradient from the front to the back of the soil cap. Much more detailed experiments using flash X-rays such as those of Bergeron 1998 would be very useful in this respect. Therefore, in the absence of any other information, it is assumed that the velocity gradient is linear.

Figure 10 shows a pressure vs time trace for a HoT of 20 mm. Initially, the pressure is due to the impact of the soil cap on the target (the end of the Kolsky bar). At first, starting about t = 0.144 ms, the pressure rises slowly, presumably due to precursor effects mentioned above. Then the pressure rises rapidly and essentially linearly, due to the impact of the soil cap, until a region of reduced density in the soil cap is encountered, after which the pressure again rises rapidly and essentially linearly to a peak. The pressure then falls rapidly a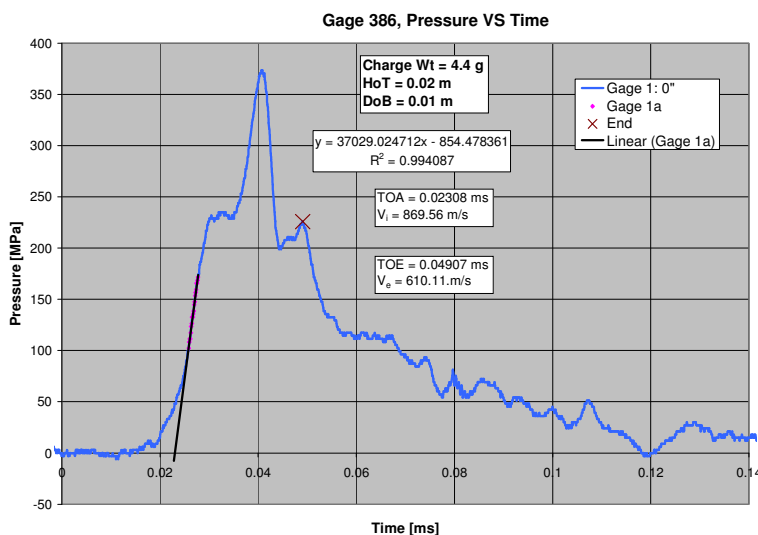s the impact phase ends, marked by the X, with a brief secondary impact. The impact phase is assumed to be over at this time. The pressure then falls rapidly to about 132 mPa, the presumed pressure of the explosion gasses expanding under the target. The subsequent declining pressure on this Kolsky bar is presumed to be due to the declining pressure as this gas expands.

Figure 10 Test Gage 386 Pressure on Target vs. Time

The pressure vs time data discussed here came from tests conducted with 4.4 g charges at a DoB of 0.01 m and HoTs of 0.02 m and 0.04 m. For

reference, this DoB and a HoT = 0.02 m scale to a DoB = 0.102 m (4 in.) and a HoT = 0.203 m (8 in.) for a 4.54 kg (10 lb) charge. The scale factor is 10.1 in this case.

In Figure 10, a straight line is fitted to the essentially linear portion of the pressure rise to estimate the ToA of the soil cap. This gives and estimated ToA = 0.02308 ms. The X shows the estimated end of the impact phase at 0.04907 ms, i.e., the arrival of the bottom of the soil cap. The impact phase is thus estimated to have lasted about 0.026 ms. The ToA and the HoT give an initial impact velocity of 869.4 m/s. The estimated time of the end of the impact phase gives a velocity of 610.9 m/s for the bottom of the soil cap. Clearly there is a velocity gradient in the soil cap which implies that the thickness has increased. The velocity gradient is assumed to be linear, as noted above. Knowing both the pressure on the target and the velocity of the material causing the pressure as a function of time, we can calculate the density of the material hitting the target as a function of time using Bernoulli's equation. Figure 11, below, shows the density of the material as it hits the target as a function of time. It has fallen significantly below its *in situ* value of 1970 kg/m.
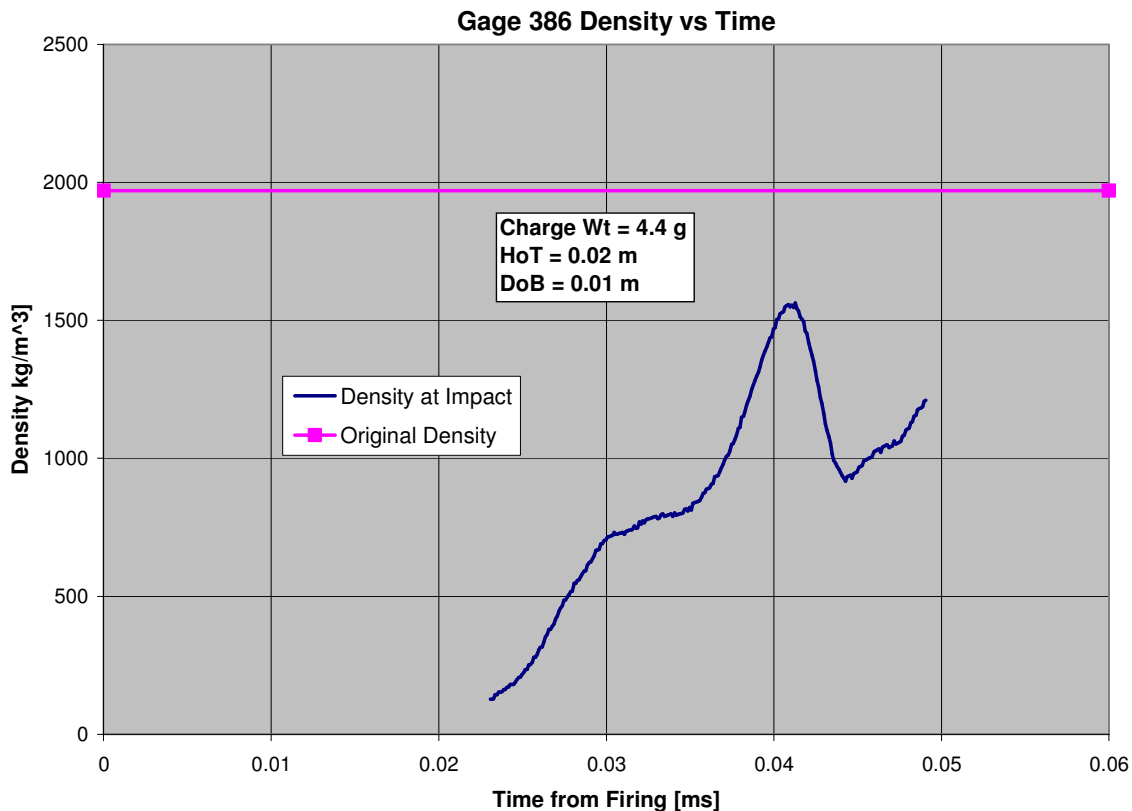
Figure 11 Test Gage 386 Soil Cap Density Impacting Target vs. Time

An assumption that the density distribution does not change during the course of the impact phase is less obviously supportable than the assumptions above, but it is not entirely unreasonable. The duration of the impact is about 0.026 ms. The speed of sound in the fully saturated *in situ* sand – water mixture, is about the same as that in water: 1497 m/s, so if this were the speed of sound in the soil cap at impact, the stress wave from the impact would reach the back of the soil cap in 0.0106 ms, well before the end of the impact. However, the speed of sound in the cavitated, reduced density, region of the soil cap is much lower, so it is not obvious

that the start of the impact will significantly change the density of regions further back in the soil cap. If one assumes that the density distribution in the soil cap does not change significantly during the impact phase, then the density distribution at the time the top of the soil cap hit the target was as shown in Figure 12. The density is everywhere lower than the *in situ* density, and the soil cap has grown in thickness from 10 mm to about 15.9 mm as a result of cavitation and the reduced density.
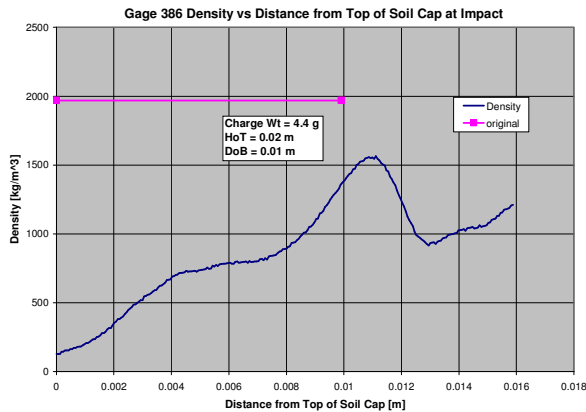
Figure 12 Density vs Distance from Top of Soil Cap at Start of Target Impact
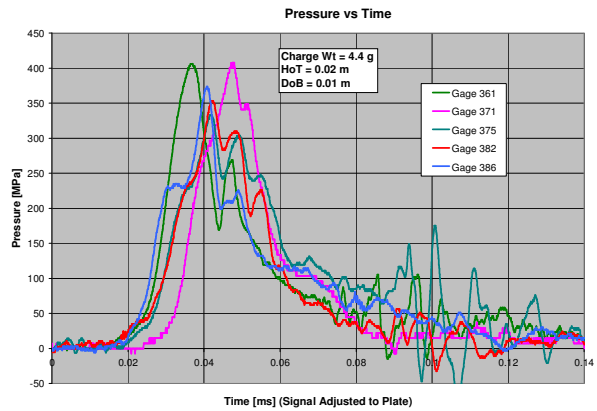
Figure 13 Pressure on Target vs Time, Five Tests – HoT = 0.02 m, DoB = 0.01 m
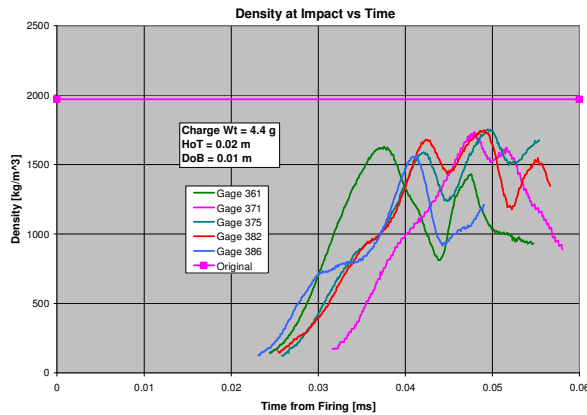
Figure 14 Density at Impact vs Time, Five Tests - HoT = 0.02 m, DOB = 0.01 m
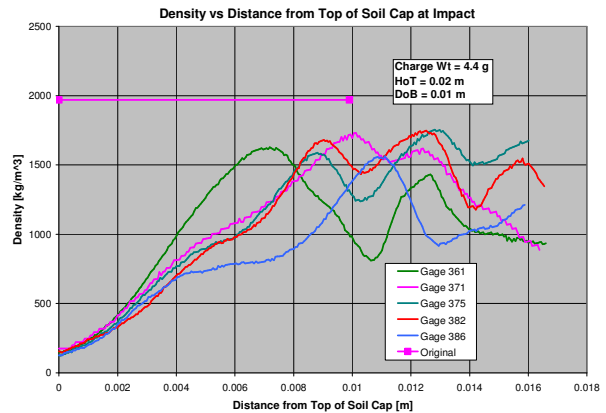
Figure 15 Density vs Distance from Top of Soil Cap at Start of Impact, Five Tests

Figure 13 shows the pressure vs time curves from four additional tests. Figures 14 and 15 show the calculated density of the material hitting the target vs time and the presumed density distribution in the soil caps at the time the tops of the soil caps hit the target. The maximum densities of all the soil caps at impact are roughly the same, about 1660 kg/m^3. The durations of the impact events in three of the cases are about 0.030 ms and in the other two cases, the duration is about 0.026 ms. This difference is not believed to be significant. While in four of the cases there is little or no trace of cavitation in the initial impact, in the Gage 386 test, there is a very clear indication of a reduced density region interrupting the initial pressure rise. In all five cases, the density shows a dip and then a rise between the peak pressure and the end of the impact

phase, indicating a region of lower density in this region of the soil cap. The ToA in the Gage 371 test is clearly later than the in the other four tests. It is not possible to be certain, but this could be because the charge was buried slightly deeper than in the other tests. The effect of this is discussed later.

The *areal density* is defined here as the mass of soil per unit area above any point on the centerline of the soil cap. Thus, at any point on the centerline of the soil cap, it is the integral of the density from the top of the soil cap to that point. It is a measure of the amount of soil above a given point on the centerline of the soil cap. In the pre-test condition, this is assumed to be a straight line as shown in Figure 16, i.e., the density does not vary with depth. Figure 16 also shows the areal density as a function of distance from the top of the soil cap for these five tests. Except for the Gage 386 test, the curves are quite similar and all end at a value that is somewhat less than the original areal density. There is less material between the front and the back of the soil cap than before the test, even though the soil cap is thicker. During this phase of the explosion event, as noted above, there are two competing processes that affect the thickness of the soil cap: thickening due to cavitation hence reduced average density, and thinning due to spherical spreading as the soil cap rises and increases in surface area. Some of the soil moves off the centerline, which is the only location considered here.
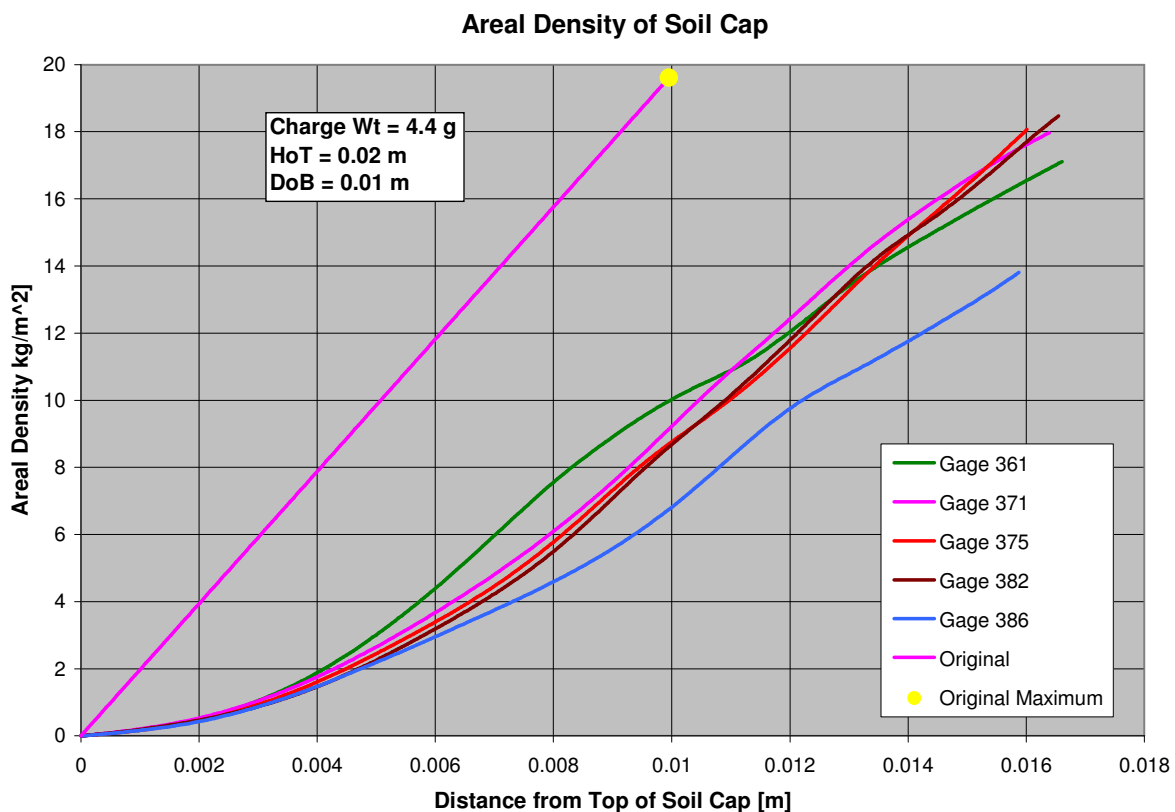

Figure 16 Areal Densities vs. Distance from Top of Soil Cap at Start of Target Impact

Figure 17 shows the pressure on the target vs. time for four tests in which the HoT was 40 mm, double that of the above tests. All other test conditions were the same. The peak pressures, on the whole, are only slightly different than before. The ToA is, of course, later since the target is

farther from the surface of the soil, and the shapes of the curves are quite different. Figure 18 shows the density of the material hitting the target as a function of time. Any cavitated regions that may have earlier existed in the soil cap have generally completely closed. In the Gage 290 test, there is evidence of a region of somewhat increased density late in the impact. The reason for this is not known. This target is being hit with a reasonably dense, but apparently somewhat thinner mass of soil. In this case, the duration of the impact event appears to be 0.017 to 0.024 ms (avg., 0.021 ms). When the HoT was 20 mm, the duration of the impact was 0.026 to 0.031 ms (avg., 0.029 ms), almost 40% longer.
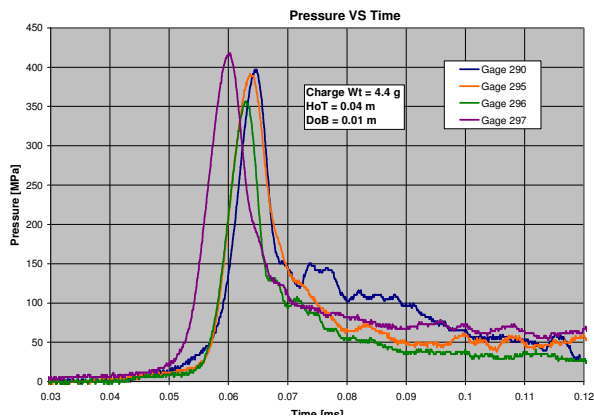
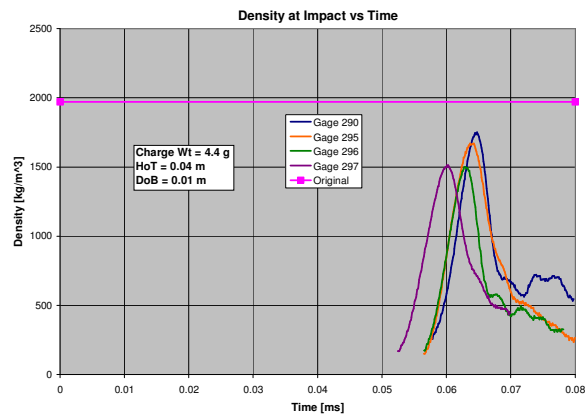Figure 17 Target Impact Pressure vs. Time, HoT = 0.04 m, DOB = 0.01 m

Figure 18 Density at Impact with Target vs. Time, HoT = 0.04 m, DOB = 0.01 m
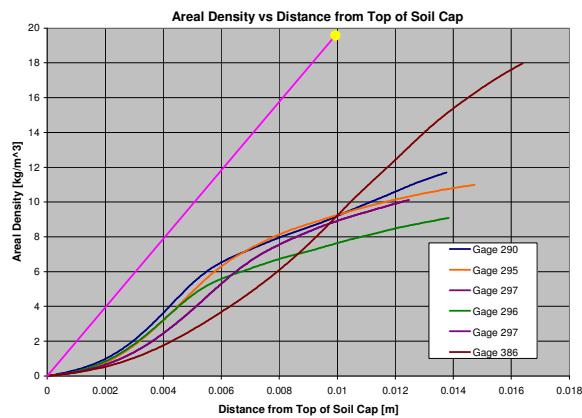

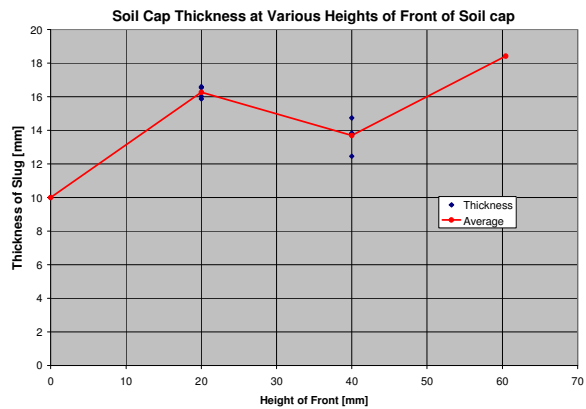Figure 19 Areal Density in Soil Cap Center at Start of Target Impact

Figure 20 Soil Cap Center Thickness at Various Heights above Original Surface

Figure 19 shows that these areal densities are not only lower than the original values, they are, in the end, lower than when HoT = 20 mm. Less soil is hitting this location on the target. This is the result of thinning of the soil cap due to hemispherical spreading of the soil cap as it rises. The distribution of the density through the soil cap is quite different. The density of the soil is higher toward the top of the soil cap and lower toward the bottom than it was earlier.

Figure 20 shows the thickness of the soil cap as a function of distance from the original top of the soil. It indicates that the soil cap quickly increases in thickness, due to bulk cavitation and

then, perhaps, decreases slightly in thickness, presumably due to spherical spreading. However, at this time there is a very limited amount of data available, including just one data point at the 60.5 mm height, so it is difficult to say more than: for the cases considered here, the soil cap thickness quickly increases and then seems to stay at about that thickness ± 2 mm. More work is needed.

Note that the method described here to determine the thickness of the soil cap is quite sensitive to the calculated value of the impact velocity. Since velocity enters the Bernoulli equation raised to the second power, small errors in its value can result in larger errors in the calculated density. For example, a ± 5% error in the velocity of the soil cap at the time it hits the target can result in an error of about ± 10 % in the calculated value of the density. The impact velocity used here is calculated as the HoT/ToA. The ToA can usually be found reasonably accurately from the pressure vs. time data. The HoT can also be measured with good accuracy when the experiment is set up. However, the ToA also is quite sensitive to the DoB of the charge. The DoB affects the mass of soil that must be accelerated by the expanding gas from the explosion and therefore the timing of the initial impact of the soil with the target. Since soil is not transparent, the DoB can be quite difficult to be certain of as the experiment is being set up. This then puts a high premium on precision and skill in setting up the experiment if the data are going to be used to determine the density in the soil cap. (The case is quite different when one wishes to measure the total vertical impulse: It is quite *insensitive* to the DOB. Taylor 2007, Fourney 2005)
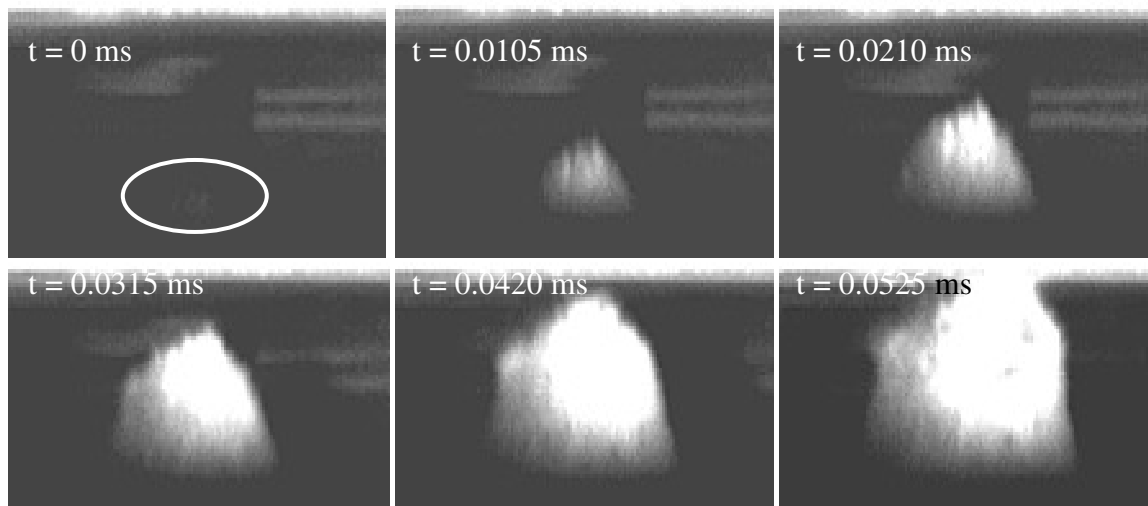

Figure 21 Test "Gage 321" Soil Cap Position at Various Times (The flash from the detonation of the charge is barely discernable within the ring in the t = 0 frame.)

A test (Gage 321) has been conducted in which a 4.4 g charge was buried 10 mm deep and the rise of the soil dome was photographed from the side at 0.0105 ms intervals as shown in Figure 21, above. Figure 22 shows that the upward velocity of the dome decreases with time, and hence with the distance traveled. Thus calculating the impact velocity as HoT/ToA somewhat over-estimates the actual impact velocity, giving a somewhat lowered estimate for the absolute values of the density of the soil cap. This does not, however, affect the calculated *form* of the distribution of density in the soil cap.
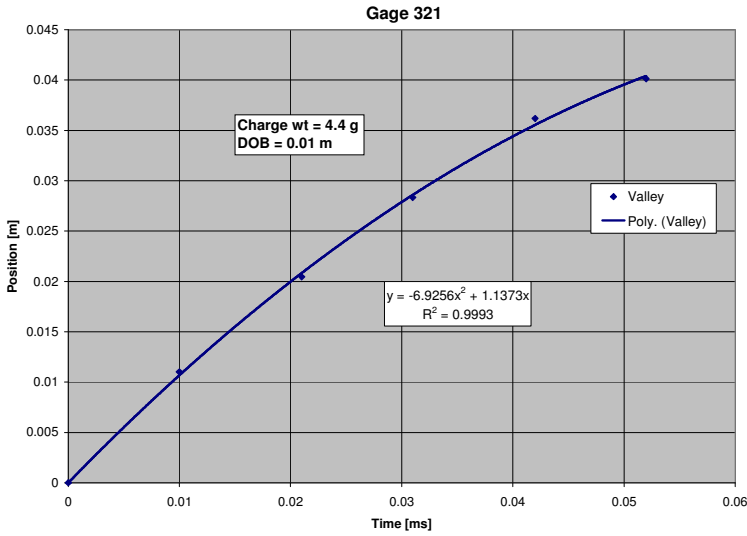
Figure 22 Test Gage 321 Position of Soil Cap vs. Time

STATISTICAL VARIATION OF TARGET LOADING

As suggested in Figures 8 and 13, above, there is a significant element of randomness in the peak pressure at any given location on the target. Even when all of the dimensions of the explosive and explosive – target geometry are kept constant, pressures measured on the target are not truly repeatable. This lack of repeatability not only causes significant shot – to – shot variation in the pressures measured at any given point; the peak pressures are not even axially symmetric within a single shot Taylor 2008.
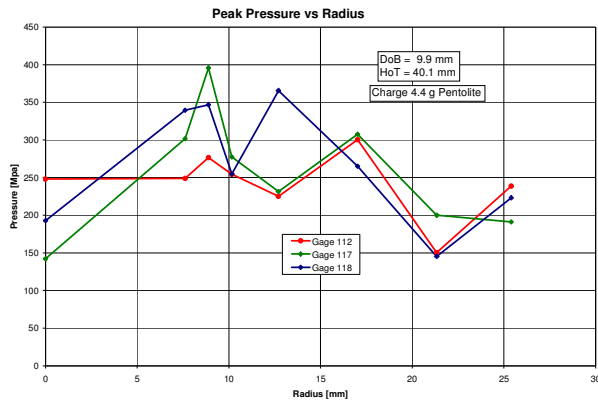

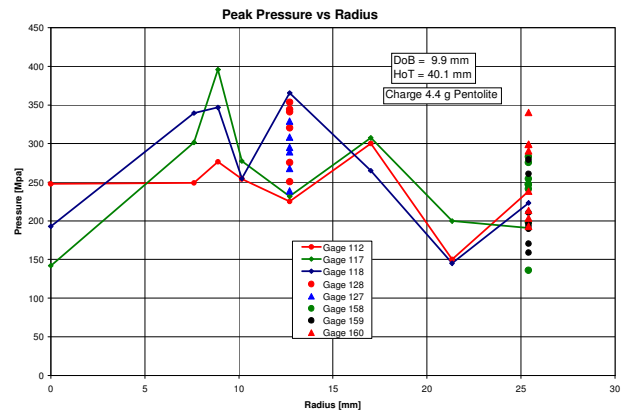Figure 23: Peak Press vs Dist from Charge Center

Figure 24 Peak Press vs Distance from Charge, With Data from Circles of Gages

Figure 23 shows the variation of the local peak pressure with horizontal distance from the center of the charge for three early tests in saturated sand with the same charge size, DoB and HoT.

The peak pressures at each gage vary significantly from shot to shot. As a result, we built targets with several gages in a circle at a constant distance from the center of the charge. Figure 24 shows the results of tests with two different rings of gages centered on the charge superimposed on the data of Figure 23. This shows that even though the total impulse transferred from an explosion to a target may be fairly repeatable, Westine 1985, the local pressures at different positions on the target surface at the same distance from the charge may vary by 50% or more in a single shot. The effect described here is not confined to saturated soils; tests conducted in drier soil have shown the same effect, Foedinger 2006.
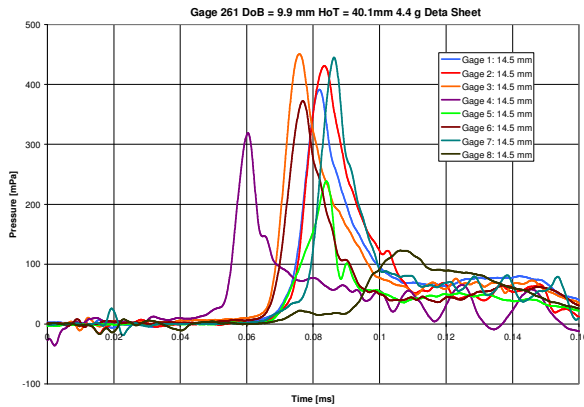

Figure 25 Typical Pressure Time Profiles

Figure 25 shows typical results obtained with eight Kolsky bars in a circle. In this case the circle had a radius (R) of 14.5 mm. These are the results obtained in a test in which the DoB of a 4.4 g charge was 10 mm. The HoT was 40 mm. As can be seen, the maximum peak pressure was 450 mPa at Gage 3 and the lowest peak pressure was 122 mPa at Gage 8. The variation in peak pressure around the circle is also irregular. There is also a significant variation in the time of arrival of the pressure pulses. The time of arrival of the peak pressure (ToP) at Gage 4 is about 0.06 ms. At Gage 8, it is nearly 0.11 ms and the rest cluster around 0.08 ms. In the discussion below, we use ToP as a measure of the time of arrival of the pressure loading. There is considerable variation in the shape of the initial pressure rise due to precursors, which makes the time of arrival of the loading somewhat unclear. However, the times of the peak pressures, especially for the gages nearest the centerline of the charge, are generally quite clear. Even so, farther from the center of the charge, the peak pressures are lower and it is more difficult to identify the peak pressure and the time of its occurrence.

The "central" set of test conditions considered here is a DoB = 10 mm and a HoT = 40 mm. In the tests at these conditions, pressure measurements were made at the radii shown in Table I. Similar data were also obtained at two other HoTs: 20 mm and 60.5 mm, with the same DoB: 10 mm. These latter two sets of tests, unfortunately, did not include tests at R = 10.1 mm. As above, in all these tests, the charge had a mass of 4.4 g and a diameter of 21.8 mm.

Table I shows the number of valid data points at each combination of HoT and R for these tests. There was a total of 506 data points. The data points at R = 0 mm, in Table I are completely independent of each other. Each comes from a separate test. In the case of the other radii, this is not the case. Four, seven or eight data points were gathered in each individual test. However, given the randomness of the data at each of the data points at the same radius from the centerline of the charge within a given test, all of the data values at each radius were treated as though they were, in fact, statistically independent of each other.

	Radius (R) (Distance to gage) [mm]								
HoT [mm]	0	10.1	14.5	25.4	31.0	39.1	50.8	63.5	76.2	Total
20	13	0	14	14	14	17	14	4	0	90
40	30	16	25	38	40	34	34	39	39	295
60.5	18	0	20	19	21	14	14	14	13	211

Table I Valid Data Points, 4.4 g Charges

In Figure 26, the blue line shows the mean of the peak pressure as a function of the distance from the center of the charge out to R = 76.2 mm for a HoT = 40 mm. (The red line on the horizontal axis shows one, two and three charge radii from the centerline of the charge.) The highest measured peak pressure does not occur at the center, but rather just beyond one charge radius from the center of the charge. The lighter lines show the bounds of one standard deviation from the mean. Figure 26 also includes the mean peak pressures for HoT = 20.0 mm and 60.5 mm. Not surprisingly, the peak pressures are higher for the target nearer the explosion and lower for the target farther away, at least close to the charge centerline. However, it is interesting that in all three cases, the mean peak pressures are much the same in the vicinity of 31 mm (~2.8 charge radii) from the centerline and beyond. It has been shown, Taylor 2008, that, under these conditions of HoT, DoB and charge mass, there is a change in the target loading mechanism at approximately this distance from the centerline of the charge. It cannot reasonably be expected that the peak pressures beyond 31 mm will remain the same as the HoT is indefinitely increased, but it does suggest that, in this region, the mean peak pressures are not terribly sensitive to HoT.
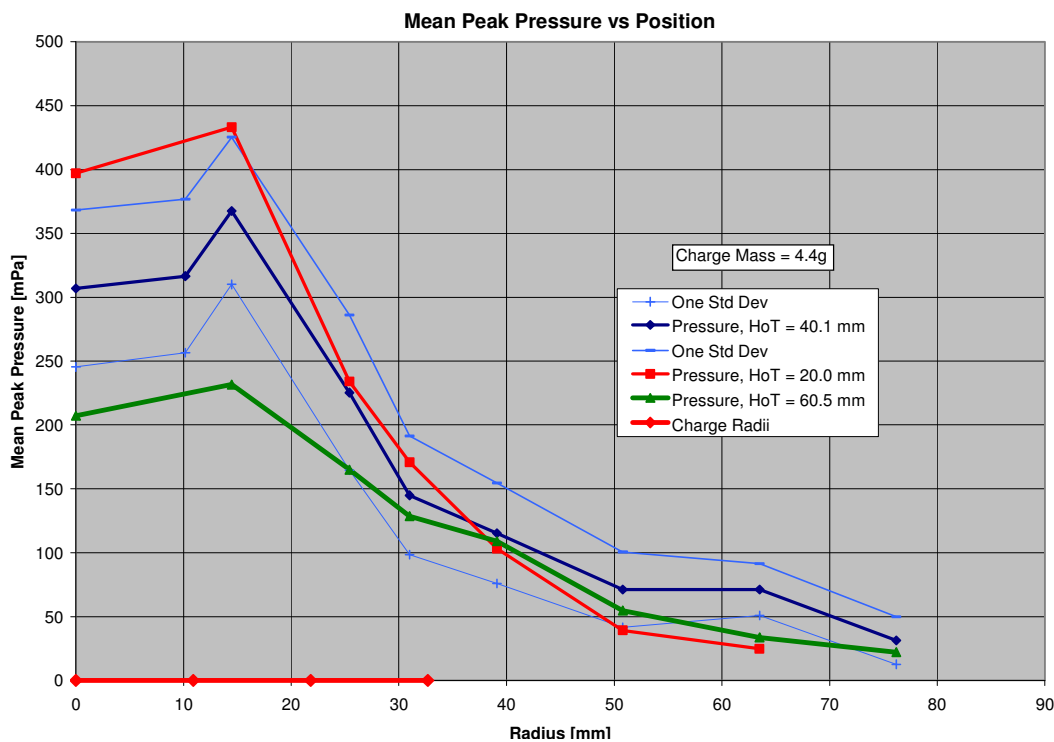

Figure 26 Mean Peak Press vs. Distance from Charge Centerline

Unfortunately, there are no data at R = 10.1 mm for HoT = 60.5 mm and 20.0 mm, which means there is some loss of detail in the graph of the mean peak pressures in this region for these HoTs. In fact, there is undoubtedly more variation in the charge – target interaction than we are able to show here, simply because of the spacing of the 6.35 mm Kolsky bars.
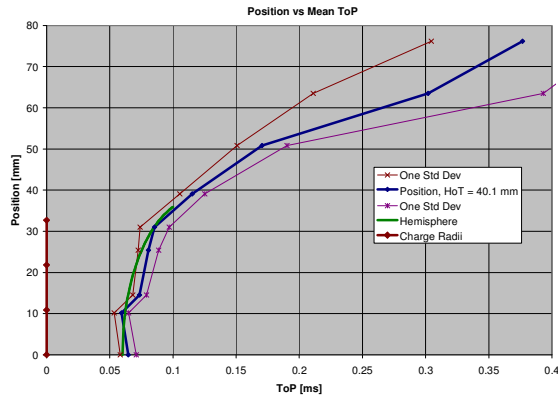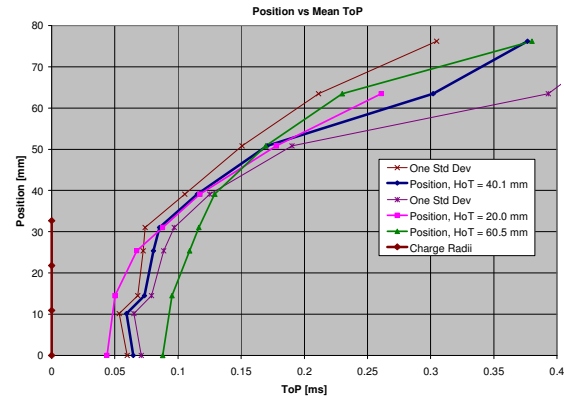

Figure 27 Position vs. ToP, HoT = 40 mm   Figure 28 Position vs ToP, HoT = 40 mm

Figure 27 shows the variation of the mean ToP with distance from the center of the charge out to R = 76.2 mm. (Note that this graph is plotted with the distance from the centerline of the charge on the vertical rather than the horizontal axis.) The lighter lines show the bounds of one standard deviation from the mean. In this case, the mean shape of the soil cap was such that the first point to hit the target was at R = 10.1 mm rather than the center. However, the time difference was very small: a 5.4 µs difference in about 60 µs. The center of the soil cap was nearly flat.

It is interesting to compare this result with the analysis in Taylor 2008. In that paper, a hemisphere (dome) of soil with a radius of 38.1 mm, about 3.5 times the charge radius, was assumed to move perpendicularly to the target, with an upward velocity equal to the HoT divided by the average time to ToP at R = 0. Figure 27 shows the times of arrival of this dome in green. While it misses some of the detail shown in the statistical data, it still appears to be a plausible simple model of the first stage of the target loading.

Figure 28 is similar to Figure 27, but includes the mean ToPs for HoT = 20 mm and 60.5 mm. As before, there are no data at R= 10.1 mm for these HoTs. Not surprisingly, the soil cap over the charge arrives earlier when the target is closer and later when the target is farther away. However the general shape of the curves is very similar at the smaller radii. A bit more surprising is that the ToPs appear to be fairly insensitive to HoT for R equal to about 31.0 mm and larger. This is the same region in which the mean peak pressures also became fairly insensitive to the HoT. As with the peak pressures, it cannot reasonably be expected that this will be the case as the HoT is indefinitely increased. This again is the region in which it has been shown, Taylor 2008, that there is a change in the target loading mechanism.

Perhaps more interesting than the shape of the mean pressure and time curves is the statistical distribution of the values and standard deviations of the peak pressures and times of arrival of the peak pressure. Figure 29 shows the cumulative distributions of peak pressures for HoT = 40

mm at each of the gage locations shown in Table I. As shown in Figure 29, the highest pressures occur at R = 14.5 mm and the pressures at R = 0 and 10.1 mm are very similar. In order to deal with these data statistically, the data were organized into "bins." The distributions were then normalized using the mean for each of the distributions, see Figure 30. Table II gives the standard deviations of the normalized pressures.
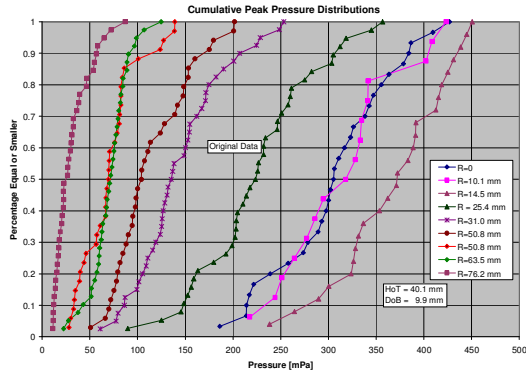

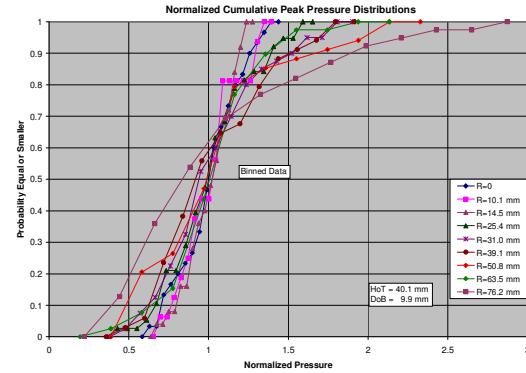Figure 29 Cumulative Peak Pressure Distributions, HoT = 40 mm

Figure 30 Normalized Cumulative Pressure Distributions, HoT = 40 mm

Radius [mm]	HoT = 20	HoT = 40	HoT = 60.5
0.0	0.1519	0.2001	0.3020
10.1	NA	0.1898	NA
14.5	0.1434	0.1567	0.2212
25.4	0.2340	0.2696	0.3455
31.0	0.3963	0.3205	0.3528
39.1	0.3450	0.3421	0.4084
50.8	0.2390	0.4144	0.3963
63.5	NA	0.2839	0.2857
76.2	NA	0.5974	0.1758

Table II Standard Deviations of Normalized Pressures

The distributions for HoT = 40 mm can be sorted into three groups based on their standard deviations. The standard deviation of the normalized pressures at R = 0, 10.1 and 14.5 are all about the same size and relatively small. The standard deviations of the normalized pressures at R = 25.4 through 63.5 mm are also similar to each other, but larger. The standard deviation of the normalized pressures at R = 76.2 mm is markedly larger than any of the others.

This suggests that we can deal with the normalized data as though there are three groups of data rather than nine: the first three constitute the first group; the next five, the second and R = 76.2 mm, the third. Figure 31 shows that the distributions for R = 0, 10.1 and 14.5 mm do indeed appear to be quite similar. The dark red curve represents the normalized data from all three locations treated as a single group. The blue curve shows that a cumulative normal distribution with a standard deviation equal to that of the grouped data (0.1809) is a good fit to the data.
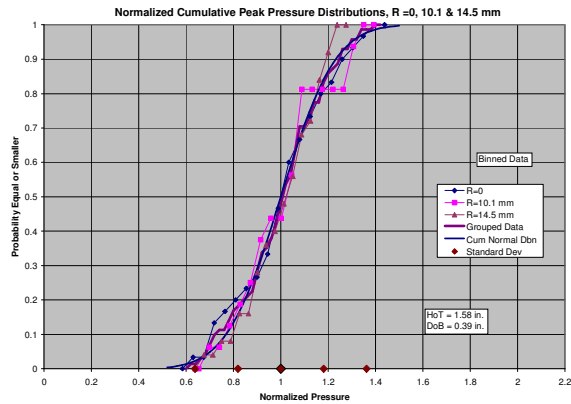
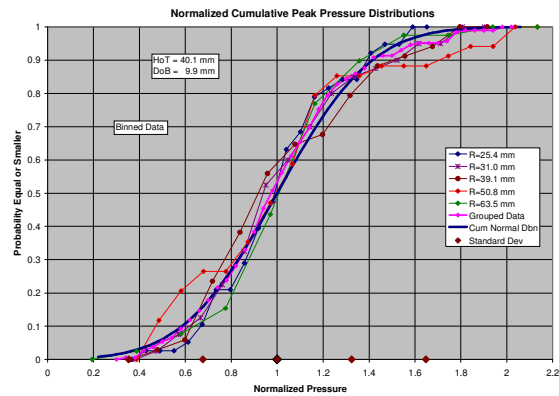Figure 31 Normalized Cumulative Pressure Distributions, R = 0, 10.1 & 14.5 mm

Figure 32 Normalized Cumulative Pressure Distributions, R = 25.4 mm and Larger

Figure 32 shows the distributions of normalized pressures for R = 25.4, 31.0, 39.1, 50.8 and 63.5 mm with the distribution of the grouped data shown in pink. When one fits a cumulative normal distribution to these data with the standard deviation of the grouped data (0.3238), this also appears to be a nice fit. The quantity of data available at R 76.2 mm is so small compared to the quantity of data available in the two above groups that this type of analysis was not applied.

Table II shows the standard deviations of the normalized pressures when HoT = 20 mm to be organized in much the same way as in the case of HoT = 40 mm: The standard deviations of the R = 0 and 14.5 mm data are similar to each other and markedly lower than those at the larger radii. The standard deviations of the normalized pressures at the larger radii are larger and at least fairly similar to each other. This suggests that the data can be handled much the same way was the data from the tests at HoT = 40 mm – treat the first two sets as a single group and treat the rest as a second group. The normalized distribution of the grouped pressures from R = 0 and R = 14.5 mm has a standard deviation of 0.1447. The normalized distribution of the grouped pressures from R = 25.4 through R = 50.8 mm has a standard deviation of 0.3051.

A similar pattern for HoT = 60.5 mm is not obvious in Table II. This is most likely because the target is farther from the surface of the soil and consequently the soil cap over the charge is more disorganized when it hits than when the target is closer. Never the less, the data were groped the same way for consistency. The normalized distribution of the grouped pressures from R = 0 and R = 14.5 mm has a standard deviation of 0.2589. The normalized distribution of the grouped pressures from R = 25.4 through R = 76.2 mm. has a standard deviation of 0.3298. As before, the standard deviation of this latter group of data is larger than the standard deviation of the data at the smaller radii, but the difference is much less.

The standard deviations of the grouped data from the inner gages are relatively small and increase with HoT: i.e.: 0.1447, 0.1809, and 0.2589, in Figure 33. This is consistent with the view that these peak pressures are impact pressures due to a hollow dome of soil hitting the target above the explosive charge, as discussed above.
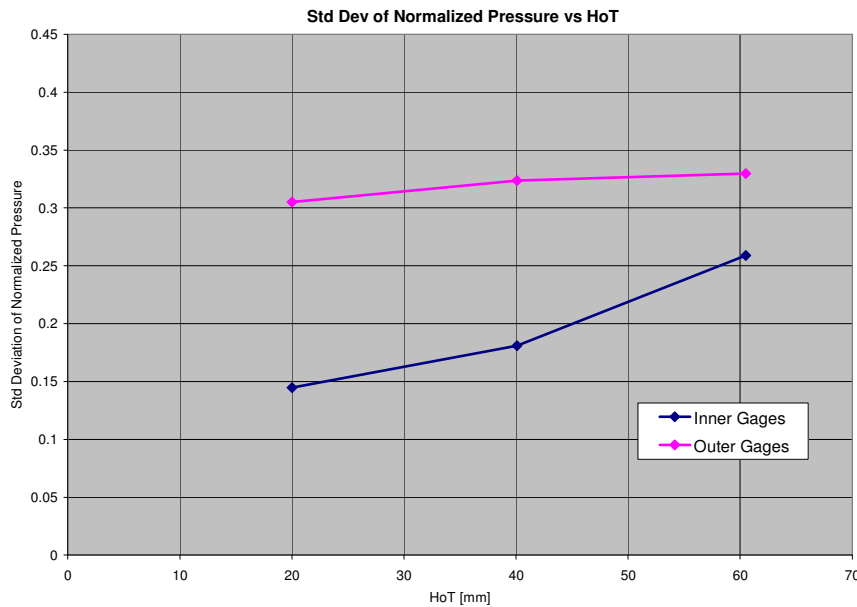
Figure 33 Standard Deviations of Grouped Normalized Pressures vs HoT

The increasing standard deviation with increasing HoT is probably due to increasing disorganization of the surface of the dome, mainly due to Richtmyer – Meshkov instability, with time and distance to the target. The standard deviations of the grouped data from the gages 25.4 mm and farther from the center of the charge are larger than those of the inner gages and relatively insensitive to HoT, ranging from 0.305 to 0.329. This suggests that these pressures are all due to the "late time" processes as described above: Soil is scooped out of the crater by the explosive gasses and forms an annular jet of material which hits the target and forms an expanding ring of stagnation pressure on it. These stagnation pressures are fairly disorganized and the disorganization appears to increase only very slowly, if at all with HoT.

The time of arrival of the loading, as represented by the ToP, also has a nondeterministic component as well as a deterministic one. Figure 34 shows the cumulative distributions of ToPs for HoT = 40 mm at each of the gage locations shown in Table I. As implied by Figure 26, the distributions for R = 0 out to R = 31.0 mm are tightly clustered with the distribution for R = 10.1 mm to the left of the others in the figure. The data at R = 63.5 and 76.2 mm show much greater scatter than at the other radii because the pressure – time traces were very noisy so that a meaningful ToP was very difficult to identify. As a result, the ToP is a poorer measure of the time of arrival of the loading at these radii. The distributions were then normalized using the mean for each of the distributions. Table III gives the standard deviations of the normalized ToPs.
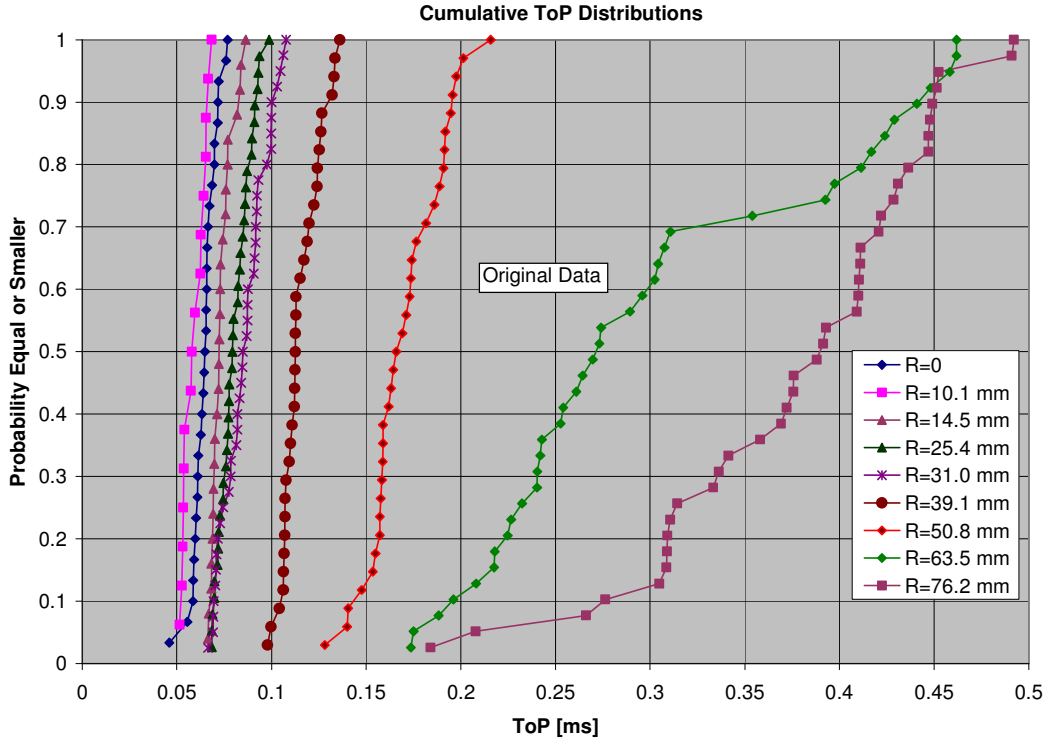
Figure 34 Cumulative ToP Distributions for HoT = 40 mm

Radius [mm]	Hot = 20 mm	HoT = 40 mm	HoT = 60.5 mm
0	0.152 5	0.0971	0.0880
10.1	NA	0.0975	NA
14.5	0.0619	0.0744	0.0953
25.4	0.0715	0.1013	0.1091
31.0	0.1126	0.1369	0.1165
39.1	0.0980	0.0860	0.1291
50.8	0.1258	0.1162	0.1694
63.5	NA	0.3010	0.2301
76.2	NA	0.1915	0.3803

Table III Standard Deviations of Normalized ToPs

The standard deviations of the ToPs are smaller than those for the peak pressures for the same groups of gages. In the case of the outer gages, this again shows that the expansion rate of the ring stagnation pressures resulting from the material being excavated from the crater is more regular than the actual stagnation pressures themselves.

The mean and standard deviation of both the peak pressure and the ToP cam be scaled using Hopkinson scaling, if the event is properly scaled, *including the diameter of the pressure measuring devices*. The diameter of the face of the pressure gage must be scaled with the scale of the event. The measured pressure is an average over the face of the pressure gage (Kolsky bar), so for the measured peak pressures to scale, the diameter of the Kolsky bar or pressure gage

must also be appropriately scaled. Taylor 2010, showed that the mean and standard deviation of the ToP scale using Hopkinson scaling. However, in this reference, there was an issue with scaling of the mean peak pressures. This has since been shown to be the result of using the same diameter, 6.35 mm, Kolsky bars regardless of the scale of the experiment, i.e., not scaling the diameter of the Kolsky bar with the scale of the event.

VISUALIZATION

As suggested by Figures 25 and 26 and shown explicitly in Figure 35, the pressure (load) on the target at the center of the loading has significantly subsided by the time a load has begun to be applied to the region farther from the center: 39.1 mm from the center in this case. Thus the target is not uniformly loaded in either position or time.
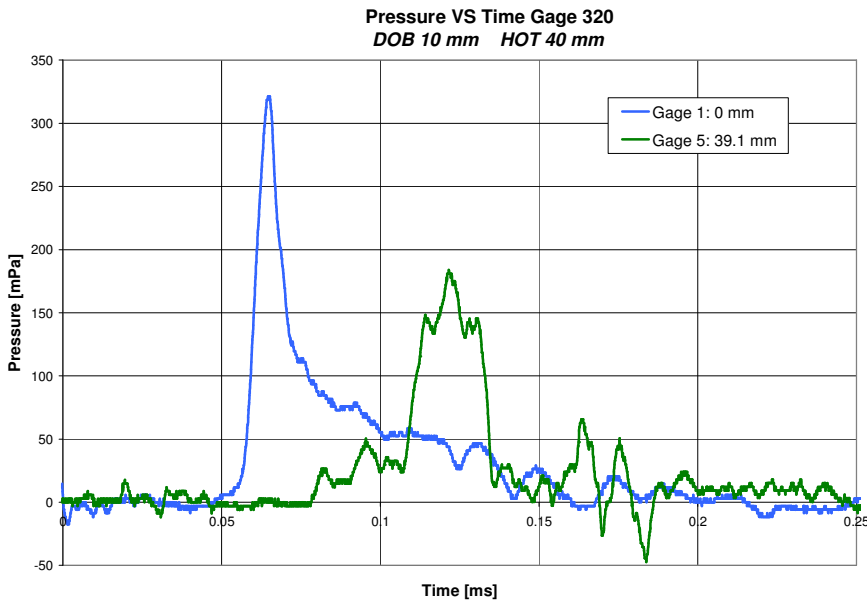

Pressure VS Time Gage 320
DOB 10 mm   HOT 40 mm

Figure 35 Pressure vs. Time: Two Different Times on Same Target

Figure 36 is a sequence of high speed videos looking through a thick, fixed Plexiglas target at a HoT of 40 mm to see its loading by a 4.4 g charge at a DoB of 10 mm. The Xs in the photos mark the positions usually occupied by Kolsky bars. There are, in fact, two Xs at each location, one on the top of the target and one on the bottom, directly b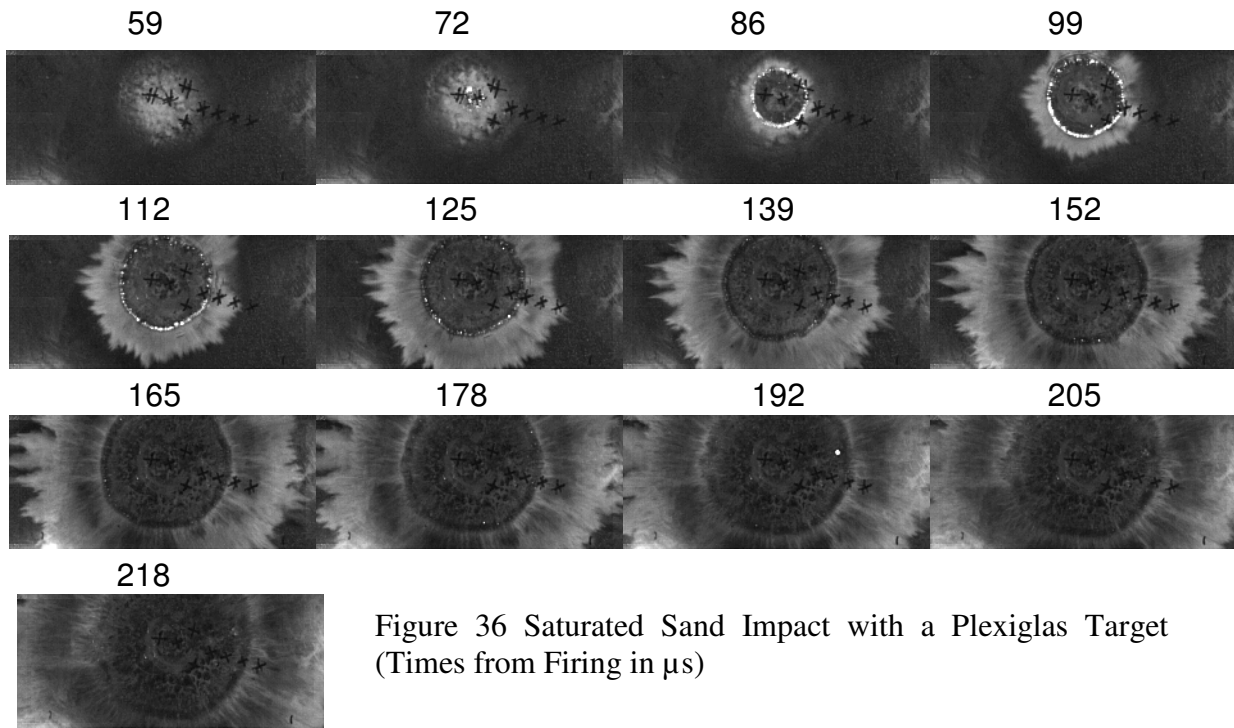elow it. In the figure one can see the rising dome of saturated sand 59 µs after firing. It is just starting to hit the target at 72 µs. In the frames at 86 µs and subsequently, it shows a ring expanding across the face of the target. As the ring reaches each of the notional Kolsky bar locations, it erases the X from the bottom of the target. At first, the ring is quite bright due to the high impact pressure, which causes ionization of the air at that location. The ring eventually dims as the impact pressures fall with time and increased radius.

Figure 36 Saturated Sand Impact with a Plexiglas Target (Times from Firing in µs)

Note in the frame at 192 µs, a bright spot has appeared, indicating a high pressure impact on the target, inside the expanding ring of the material being excavated from the crater and hitting the target. Had there been a Kolsky bar at this point, one would have seen pressure spike with no indication of why the spike had occurred this late in the event.
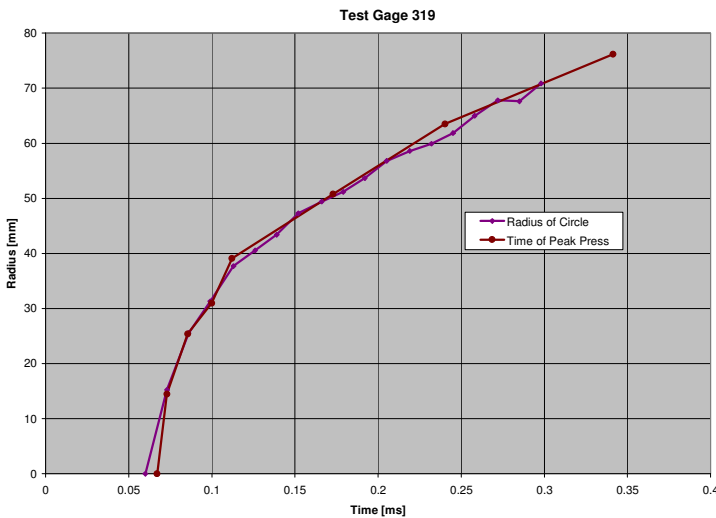

Figure 37 Visual and Pressure Data Compared

In Figure 37 the radius of this expanding ring as a function of time is compared with the ToP in a single test in which pressure measurements were made and the loading was similarly visualized. It shows that the expanding ring shown in Figure 36 is indeed the instantaneous location of the peak pressure on the target plate. The radius of this annulus of peak pressure increases with time, as shown. However, the *rate* of increase in the radius decreases rapidly with time. From a radius of 37.7 mm to a radius of 70.9 mm, the velocity at which the radius of the peak pressure increases slows from about 455 m/sec to about 240 m/sec. The thickness of this annular stream of material hitting the target also increases as its radius increases which manifests its self as a broadened pressure vs. time curve.

SUMMARY

This paper has shown some of the ways in which small scale testing may be used. It has been especially useful in exploring the details of the target loading mechanisms. We have been able to show that, in general, if the target is of reasonable size relative to the charge, the target is loaded in two steps or phases. In the first phase, the target receives a very concentrated, very localized load by the cap of soil over the buried charge. This is then followed by less intense loading spread over a larger area and a longer time. In this second phase, the load is, to some extent, concentrated in an expanding, and thickening, ring on the target. It has been possible to gain insight into the density distribution in the soil cap that provides the first phase of the target loading. This is expected to be quite useful in validating computational models of the loading.

The actual load on a target by the explosion of a buried charge has a significant non-deterministic element. We believe that only through small scale testing is it possible to conduct enough nominally identical tests to develop sound estimates of the nondeterministic part of the target loading. Fortunately, it appears that both the mean and the standard deviation of this loading are scalable to larger charge sizes.

ACKNOWLEDGEMENTS

REFERENCES

Bergeron, D., Walker, R., Coffey, C., *Detonation of 100-Gram Anti-Personnel Mine Surrogate Charges in Sand*, Defence Research Establishment Suffield Report No. 668, 1998

Foedinger, R., Caiazzo A., *Methodology for Improved Characterization of Land Mine Explosions*, MSC TPR 6062/CC02, Material Sciences Corp., Horsham, PA, Aug 2006

Fourney W. L., Taylor L. C. and Robeson D., "Underwater Cratering and Channeling With Explosives", *Fragblast*, Vol. 3, No. 2, pp. 65-183, 1999

Fourney W.L., Leiste H.U., Bonenberger R. & Goodings, D.J., "Mechanism of Loading on Plates Due To Explosive Detonation", *Fragblast*, Vol. 9, No. 4, 2005, 205 – 217

Palekar, A., Vorobieff, P., and Truman, C. R., "Two-dimensional Simulation of a Shock-accelerated Gas Cylinder," *Progress in Computational Fluid Dynamics*, 2007, Vol. 7, No. 8, pp. 427-438

McAndrew, B., Kukuck, S., Hernandez, V., Skaggs, R. R.. "Analysis of Data Compiled from Flat Plate Experiments Performed at the U .S. Army Research laboratory Vertical Impulse Measurement Facility," *Proceedings of the 2007/2008 Warheads and Ballistics Joint Classified Symposium,* 12 -14 Feb 2008, Monterey, CA

Snay, H. G. and Kriebel, A. R. *Surface Reflection of Underwater Shock Waves*, NOLTR 70-31, 1970 U.S. Naval Ordnance Laboratory, White Oak, MD

Taylor, L. C., Leiste, H. U., Fourney, W. L., "Pressures on Targets from Buried Explosions," *Blasting and Fragmentation*, 2010, Vol. 4, No. 3, pp 165-192

Taylor, L. C., Szymczak W. "Platform Loading from Explosions in Saturated Sand Using a Visco-Plastic Model, *Blasting and Fragmentation*, V 1, No 1, Sept 2007, pp 51-68

Taylor, L. C., Fourney, W. L., Leiste, H. U., Cheeseman, B.; "Loading Mechanisms on a Target From Detonation of a Buried Charge" *Proceedings of 24th International Symposium on Ballistics*, New Orleans, LA, 22 - 26 Sept 2008

Taylor, L. C., Fourney, W. L., Leiste, H. U., "Soil Cap Density Distributions Resulting From Buried Explosions in Saturated Sand,", *Blasting and Fragmentation*, 2011, Vol. 5, No 2, pp 73 – 86

Westine, P.S., Morris, B.L., Cox, P.A., Polch, E. Z., *Development of a Computer Program for Floor Plate Response from Land Mine Explosions*, Contract Report No. 13045, U.S. Army TACOM Research and Development Center, Jan 1985